Journal of Power Sources 196 (2011) 5191–5196

Contents lists available at ScienceDirect

Journal of Power Sources

journal homepage: www.elsevier.com/locate/jpowsour

Fabrication of a thin walled β″-alumina electrolyte cells

Amin Mali*, Anthony Petric

Department of Materials Science and Engineering, McMaster University, Hamilton, Ontario, Canada L8S 4L7

ARTICLE INFO

Article history:
Received 22 December 2010
Received in revised form 3 February 2011
Accepted 4 February 2011
Available online 12 February 2011

Keywords:
Sodium/nickel chloride battery
β″-Alumina electrolyte
Internal resistance
Porous substrate
Slip casting

ABSTRACT

Dense β″-alumina electrolyte tubes with thickness less than 50 μm were slip cast on a porous substrate of β″-alumina. The resistance of the composite electrolyte was measured by a DC method. The area specific resistance of a thin layer electrolyte versus the full thickness electrolyte was lower by a factor of 1.6. The components of cell resistance were determined. It was concluded that interfacial resistance is a dominant factor in the electrolyte resistance.

© 2011 Elsevier B.V. All rights reserved.

1. Introduction

The $Na/NiCl_2$ battery shows promise for powering electric vehicles and load leveling systems. The $Na/NiCl_2$ cell (Fig. 1), with an optimum temperature range of 260–350 °C, contains a liquid sodium negative electrode separated from the positive electrode by a sodium ion conducting β″-alumina solid electrolyte [1–3].

The β″-alumina electrolyte contributes approximately 50% of the total cell resistance at full charge. The electrolyte resistance has been decreased to some extent via replacing the cylindrical electrolyte by a clover leaf shaped electrolyte [4]. However, the greatest improvement can be achieved by reducing the thickness of the current solid electrolyte from 1–2 mm to 10–50 μm which results in a significant decrease in solid electrolyte resistance.

Fig. 2(a) and (b) illustrates the standard β″-alumina electrolyte in comparison to the concept of the new electrolyte design. The objective is to fabricate dense electrolyte tubes with reduced thickness of less than 100 μm and supported on a porous substrate that allows the easy mass transport of liquid sodium through pore cavities.

Slip casting was found to be the most convenient method to fabricate such thin electrolytes. The optimized slip casting parameters and sintering conditions are described. The components of cell resistance and effect of the electrolyte thickness on the cell resistance also will be discussed.

2. Experimental procedures

2.1. Slip casting

Two types of β″-alumina powders used in electrolyte fabrication were supplied by Ceramatec Inc. (CMT-β″) and MES-DEA Inc. currently called as FZ SoNick (MES-β″). Carbon powder (Grade 4023) supplied by Graphite Mills Inc. was used as pore-forming agent. The reduction in average particle size (APS) of starting powders was achieved by milling for 72 h with zirconia balls. The substrate slips were prepared from β″-alumina and carbon powder dispersed in water by adding 0.5 wt.% Darvan C (ammonium polymethacrylate) followed by ball milling for 24 h. The weight ratio of carbon to β″-alumina in the slip was fixed at 0.8. The slip was cast into plaster moulds, allowing a residence time of 3 min to increase the wall thickness to 1 mm and pouring out the excess. The coating slip was prepared by mixing a 90:10 ratio by weight of methanol and β″-alumina powder. The coating was applied inside the tube by pouring the slip into the tube for a time interval less than 30 s before decanting.

2.2. Sintering

Fig. 3 shows the optimized sintering process including pre-sintering in air and sintering with buffer. Pre-sintering in air involves carbon burn out at 600 °C followed by strengthening the green body at 1200 °C, at a slow heating rate of 1 °C min^{-1} and 2 °C min^{-1}, respectively.

* Corresponding author at: Department of Materials Science and Engineering, McMaster University, 1280 Main Street West, Hamilton, Ontario, Canada L8S 4L7. Tel.: +1 905 525 9140.
E-mail addresses: amin_mali@yahoo.com (A. Mali), petric@mcmaster.ca (A. Petric).

0378-7753/$ – see front matter © 2011 Elsevier B.V. All rights reserved.
doi:10.1016/j.jpowsour.2011.02.021

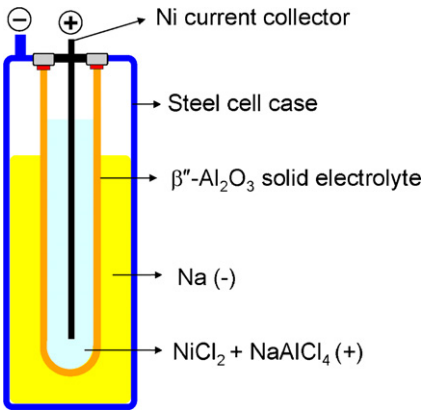

Fig. 1. Schematic depiction of $Na/NiCl_2$ cell.

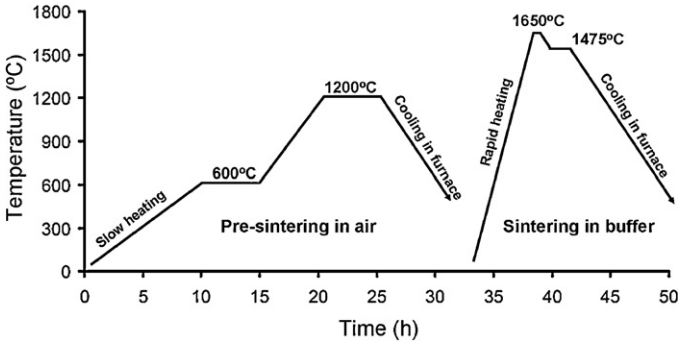

Fig. 3. The optimized sintering process including pre-sintering in air and sintering in-buffer.

In order to minimize sodium loss and prevent excess grain growth, a two step sintering procedure in a buffer of β-alumina powder and 2% by weight Na_2CO_3 was applied. The electrolyte tube was placed in a tapered α-alumina crucible and packed with buffer powder to fully cover the tube. A rapid heating rate of 5 °C min^{-1} and a dwell time of 1 h at 1650 °C were used to achieve a dense thin film electrolyte. The process included a 45 min homogenization at 1475 °C during cooling.

2.3. Characterization methods

The phase identification of powders and fabricated electrolyte was performed by X-ray diffraction (XRD) using Cu $K_{\alpha 1}$ radiation (λ = 1.54056 Å). The solid electrolyte microstructure and fracture surface were examined by scanning electron microscopy (SEM). Chemical analysis of the powders was carried out using an inductively coupled plasma-optical emission spectrometer (ICP-OES). A particle size analyzer was used to determine the particle size distribution by liquid phase sedimentation. The ASTM standard test method (C373-88) was applied to determine the bulk density and apparent porosity of the sintered products. The ultimate integrity of the β″-alumina tubes was examined by means of a liquid penetrant test. Tubes that were not dense enough to prevent liquid penetration were rejected and the ones that passed the liquid penetrant test were used to construct galvanic cells.

2.4. Conductivity measurements

The resistance of the fabricated electrolytes was measured by the DC method using galvanic cells. Fig. 4 illustrates a schematic of the Na|β″-alumina|Sn-1%Na galvanic cell and the ionic conductivity measurement apparatus which was operated inside a furnace well in an argon filled glove box. After loading the cell with high purity sodium, the cell was hermetically sealed by means of a tantalum cone and a stainless steel clamp. The Ta cone was tapped and threaded on both ends to allow attachment of Ta electrical leads; it was then clamped to the lid by a cell holder machined from a Zr–2.5%Nb alloy. The deformation of the tantalum around the annular point of contact with the α-alumina lid was sufficient to provide an impervious seal.

A DC current of 1–100 mA was applied using a PAR 173/179 galvanostat to measure the resistance of the cell at different temperatures. The cell resistance was calculated from:

$$E = E^o - iR_{total} \quad (1)$$

where E is the voltage, E^o is the open circuit voltage of the cell, i is the current, and R_{total} is the total resistance of the cell which can be described as $R_{total} = R_{int} + R_{cell} + R_{bulk}$ in which R_{int} is the interfacial resistance arising from charge transfer barrier at the electrode/electrolyte interface, R_{cell} is the electrical resistance of the cell circuit without solid electrolyte, and R_{bulk} represents the bulk resistance of the electrolyte given by:

$$R_{bulk} = \frac{L}{\sigma_{bulk} A} \quad (2)$$

where L is the electrolyte thickness, A is the electrolyte surface area and σ_{bulk} is the electrolyte conductivity. The electrolyte resistance is the sum of the interfacial resistance and the bulk resistance of the solid electrolyte ($R_{electrolyte} = R_{int} + R_{bulk} = R_{total} - R_{cell}$).

However, it was found that the resistance data obtained with this experimental setup was noticeably higher than the expected theoretical values probably due to the high interfacial resistance from the β″-alumina|Sn-1%Na interface and partial wetting of β″-alumina by liquid tin at the operating temperature of 250–350 °C.

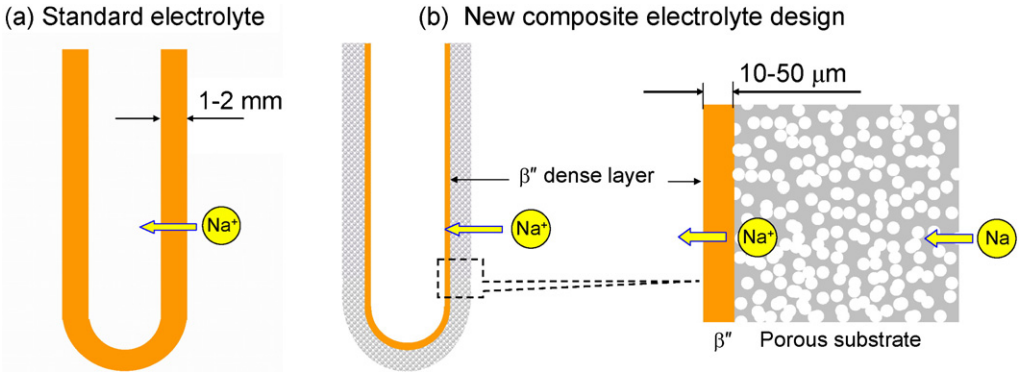

Fig. 2. Schematic representation of (a) the standard β″-alumina electrolyte in comparison to (b) the new composite electrolyte design.

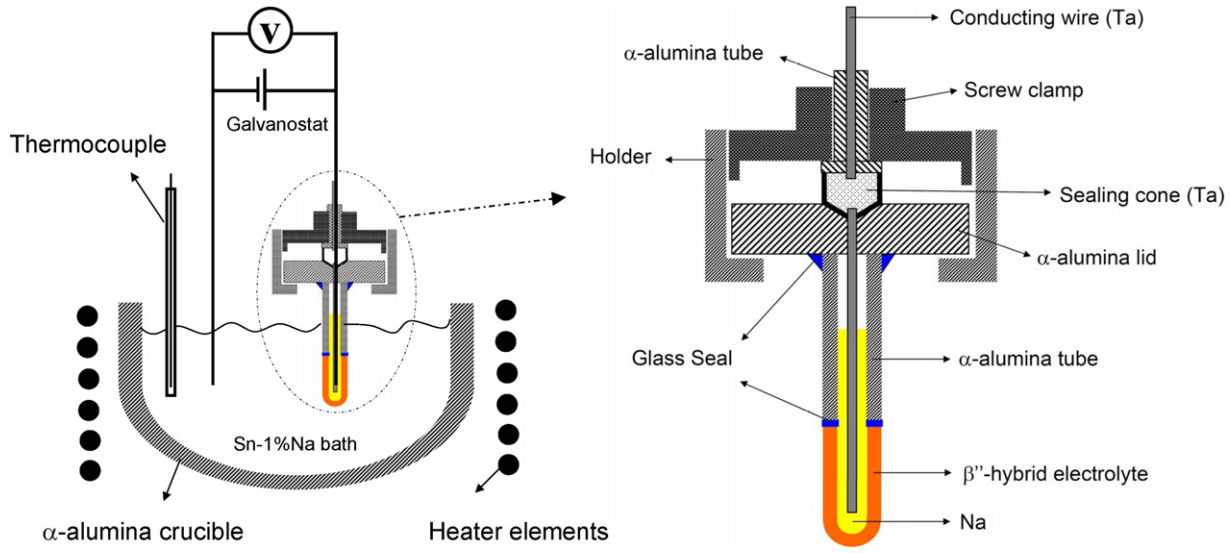

Fig. 4. Schematic of the Na|β″-alumina|Sn-1%Na galvanic cell and the ionic conductivity measurement apparatus.

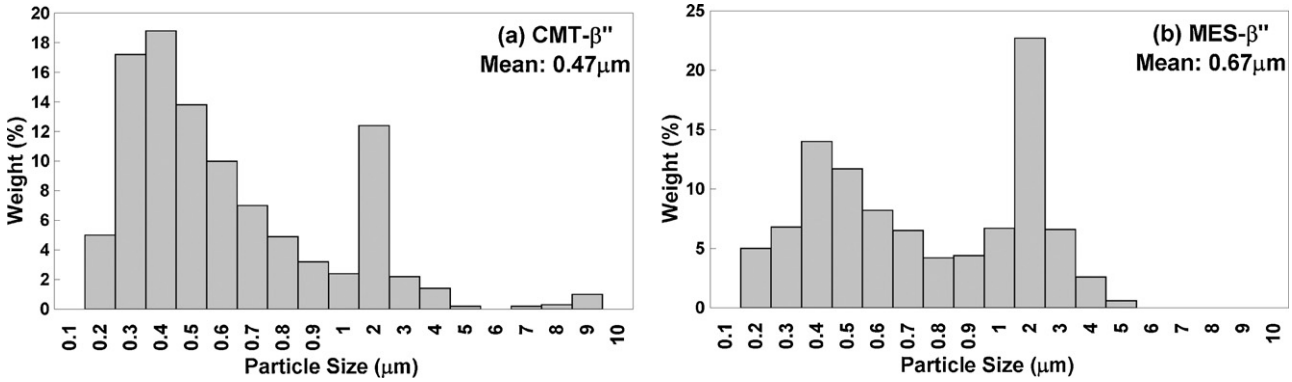

Fig. 5. Particle size distribution graphs for (a) CMT-β″ and (b) MES-β″ powders ball milled for 72 h (Note the change of scale at 1 μm.).

To circumvent this problem, the apparatus was modified and pure sodium was used as both anode and cathode.

3. Results and discussions

3.1. Electrolyte fabrication

The objective of this study was to fabricate and characterize a hybrid electrolyte composed of two layer of β″-alumina; a 1–2 mm thick porous substrate and a 10–50 μm dense coating to serve as the cell electrolyte. In the following text, reference is made to either "substrate" or "coating" layer as defined above.

The ICP chemical analysis results for the supplied powders (Table 1) shows that both powders are lithia stabilized and their compositions are nearly the same. Fig. 5 shows the particle size distribution of the powders after milling. The average particle size for both CMT-β″ and MES-β″ powders is below 0.7 μm which is a desirable size for powders used in the preparation of slips. However, CMT-β″ possesses a smaller size of 0.47 μm with 62 wt.% of particles below 1 μm.

Table 1
Inductively coupled plasma-optical emission spectroscopy (ICP-OES) chemical analysis of β″-alumina powders.

Powder	Element (wt.%)			
	Al	Li	Mg	Na
CMT-β″	50.957	0.349	0.000	6.699
MES-β″	53.505	0.307	0.005	6.685

Fig. 6 shows the X-ray diffraction patterns of the powders. Based on JCPDS powder diffraction file 25-0775 (β-alumina) and 19-1173 (β″-alumina), an estimate of the phase content (β″/β) can be made by comparing the characteristic peaks of β and β″ phases [5,6]; the intensity of the (1 0 2) β-alumina peak at $2\theta = 19.93^\circ$ is 1.5 times of the (0 0 8) β″-alumina peak at $2\theta = 20.93^\circ$. Hence, the fraction of β″-alumina, f(β″), is determined as follows:

$$f(\beta'') = \frac{1.5I_{\beta''(008)}}{1.5I_{\beta''(008)} + I_{\beta(102)}} \quad (3)$$

where I represents the relative intensities of the corresponding characteristic peaks in the X-ray diffraction pattern. None of the powders are found to be single-phase β″-alumina. A considerably higher β″ fraction (75%) is found in the CMT-β″ compared to f(β″) = 35% in MES-β″. It should be noted that a smaller value for f(β″) means a larger proportion of the β-alumina phase in the powder.

An ideal powder for the coating is the one that leads to a fully dense film whereas the optimum powder for the substrate must remain porous after sintering. Subsequently, investigating the densification behavior of different powders under sintering conditions is helpful to determine the optimum powder for the coating and the substrate. To this end, tubes of β″-alumina were cast from slips

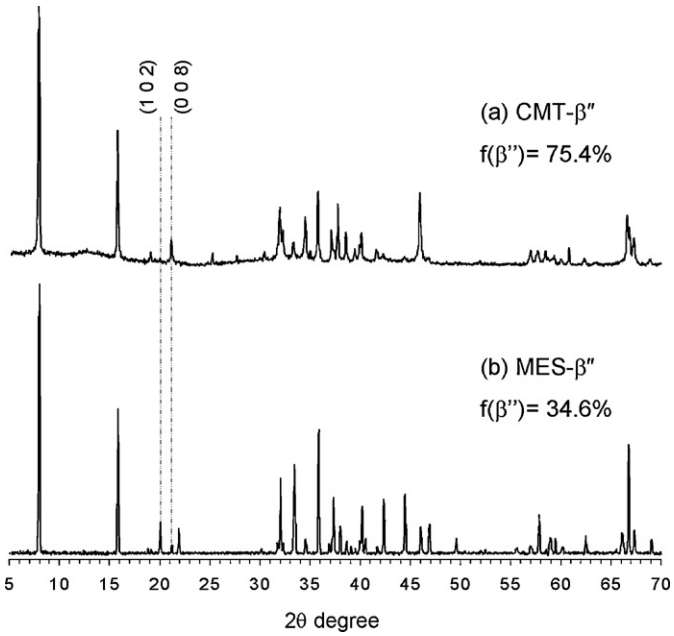

Fig. 6. X-ray diffraction patterns of (a) CMT-β″ and (b) MES-β″ powders.

without carbon and sintered in buffer at 1650 °C for 30 min. The SEM images of the fracture surface of the tubes (Fig. 7) show that one fabricated from CMT-β″ is completely dense while the MES-β″ tube possesses a high level of porosity. This is consistent with the results from the X-ray diffraction and particle size analysis. A high level of densification observed for the CMT-β″ tube can be explained by its smaller particle size and higher β″-alumina phase content compared to that of MES-β″, promoting liquid phase sintering. The porous structure of the MES-β″ can be related to its plate-like morphology with markedly elongated grains along its *a* axis coupled with a high β-alumina proportion. The former factor prevents the particles from packing well against the mould wall during slip casting and the latter hinders liquid phase sintering.

Consequently, fully dense thin film electrolytes supported on a porous substrate could be achieved by the CMT-β″ for coating and MES-β″ for the substrate via sintering in buffer at 1650 °C for 1 h (Fig. 8(a)). The apparent porosity and bulk density of the sintered product was measured to be nearly 24.6% and 2.31 g cm^{-3}, respectively.

The interior surface of the coating is shown in Fig. 8(b). Although the non-conducting *c*-axis of the β″-alumina grains in the porous substrate tend to be strongly oriented in the radial direction, the grains in the coating show a much lower degree of alignment and are more randomly oriented. This can be explained by a significantly lower capillary force existing during casting of the second layer, the coating, compared to that during casting of the substrate.

A comparison of the X-ray diffraction pattern of randomly oriented powder with those of the coating and the substrate confirms this conjecture (Figs. 9 and 10). The observed texture in the substrate and coating causes higher relative intensity for the characteristic peaks, e.g. (1 0 7), of coating and substrate compared to those for randomly oriented powders. This behavior is more significant in the substrate in which there is a higher degree of alignment.

Although such unfavorable texture also occurs during slip casting, the degree of orientation in the coating (thin film electrolyte) is negligible and does not degrade the electrolyte conductivity. This can be considered as an advantage to the other fabrication methods such as isostatic pressing which lead to a high degree of orientation that can lower the conductivity [7]. Moreover, the porous substrate improves the wetting of β″-alumina by Na covering the entire surface. The porous substrate could toughen the ceramic by stopping or deflecting microcracks at the pore surfaces. The outer porous substrate also protects the thin inner dense electrolyte.

3.2. Ionic conductivity

3.2.1. Full thickness electrolyte (1 mm)

Pressed pellets of CMT-β″ sintered in buffer at 1650 °C for 30 min (Fig. 11(a)) show a dense microstructure analogous to the one observed for the standard solid electrolyte of the Na/$NiCl_2$ (ZEBRA) battery seen in Fig. 11(b). For consistent resistance measurement, it is necessary to have samples with identical surfaces both topographically and chemically. Because sintering causes minor changes in the surface composition and topography that could affect the interfacial resistance, the sintered pellets were polished to achieve identical surfaces and remove inhomogeneities from the surface formed during sintering.

Assuming the same interfacial resistance for the same type of cells and the same bulk conductivity (σ) for two pellets of different thickness (L_1 and L_2) and same surface area (A), the various components of the resistance can be calculated:

$$\text{Measured } R_{electrolyte1} = R_{int} + \frac{L_1}{\sigma A} \quad (4)$$

$$\text{Measured } R_{electrolyte2} = R_{int} + \frac{L_2}{\sigma A} \quad (5)$$

Table 2 summarizes the conductivity measurements of CMT-β″ pellets of different thickness and same surface area at 300 °C by a Na|CMT-β″|Sn-1%Na or a Na|CMT-β″|Na cell. The data show an interfacial resistance of 3.24 Ω (1.94 Ω cm^2) for a Na|CMT-β″|Na cell which is lower than 3.60 Ω (2.16 Ω cm^2) for a Na|CMT-

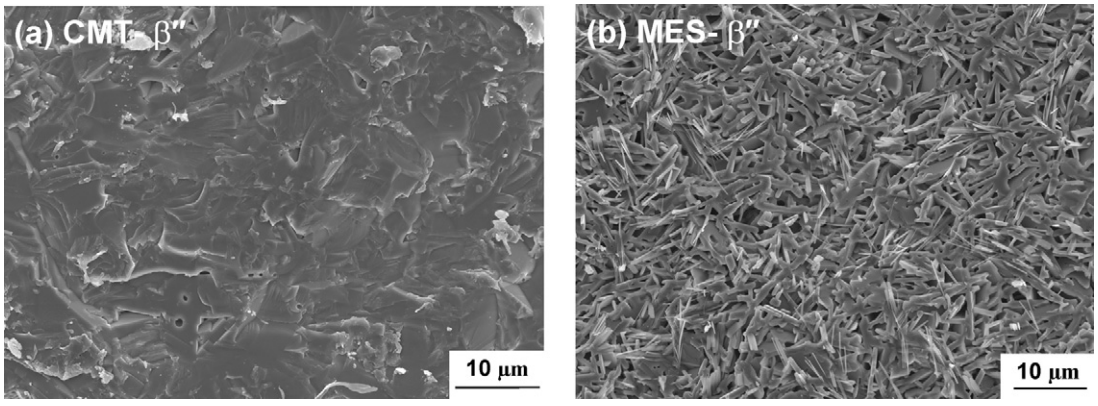

Fig. 7. SEM images of the fracture surface of cast tubes of (a) CMT-β″ and (b) MES-β″ without carbon sintered in buffer at 1650 °C for 30 min.

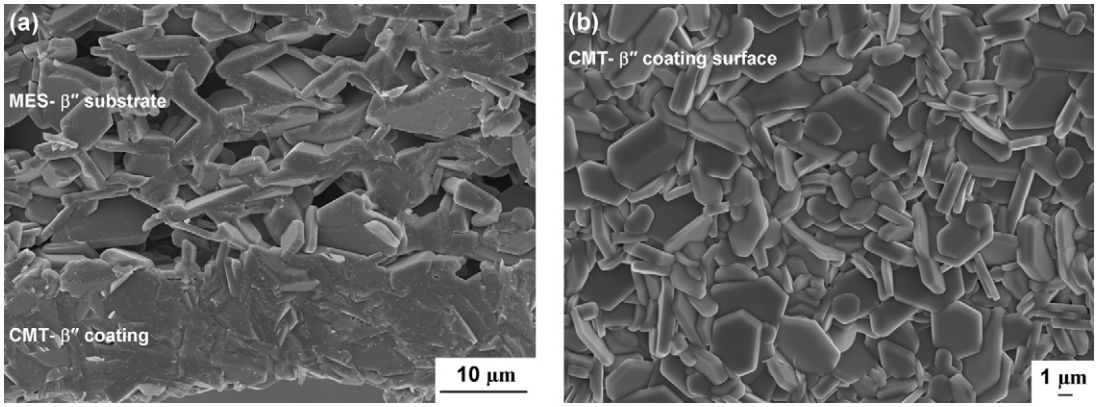

Fig. 8. SEM images of (a) fully dense thin film electrolyte of CMT-β″ supported on a porous substrate of MES-β″and (b) its interior surface sintered in buffer at 1650 °C for 1 h.

Table 2
The resistance components and the bulk conductivity for CMT-β″ pellets at 300 °C, area = 0.6 cm^2.

Cell type	Polished pellets thickness (mm)	Resistance (Ω)					σ (S cm^{-1})
		R_{total}	R_{cell}	R_{int}	R_{bulk}	$R_{electrolyte}$	
Na|CMT-β″|Sn-1%Na	1.00	5.35	0.65	3.60	1.10	4.70	0.15
Na|CMT-β″|Sn-1%Na	2.78	7.30	0.65	3.60	3.05	6.65	0.15
Na|CMT-β″|Na	1.00	4.99	0.65	3.24	1.10	4.35	0.15

R_{total}: Total resistance of the cell.
R_{int}: Interfacial resistance.
R_{cell}: Electrical resistance of the cell circuit.
R_{bulk}: Bulk resistance of the electrolyte.
$R_{electrolyte}$: Electrolyte resistance.
σ: Bulk conductivity of the electrolyte.

β″|Sn-1%Na cell. This could be explained by higher resistance at β″-alumina|Sn-1%Na interface than that at β″-alumina|Na interface due to the better wetting of β″-alumina by liquid sodium compared with liquid tin. Fig. 12 shows the interfacial resistance of CMT-β″ pellets in a Na|CMT-β″|Sn-1%Na cell as a function of temperature. As expected, the interfacial resistance decreases with increasing temperature due to an increase in diffusion rate.

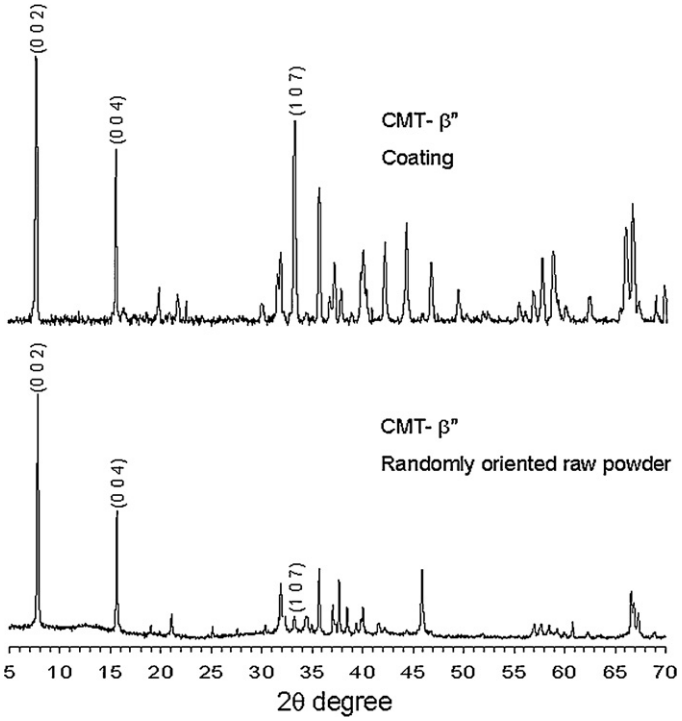

Fig. 9. Comparison between the X-ray diffraction patterns of CMT-β″ powder and cast as the coating.

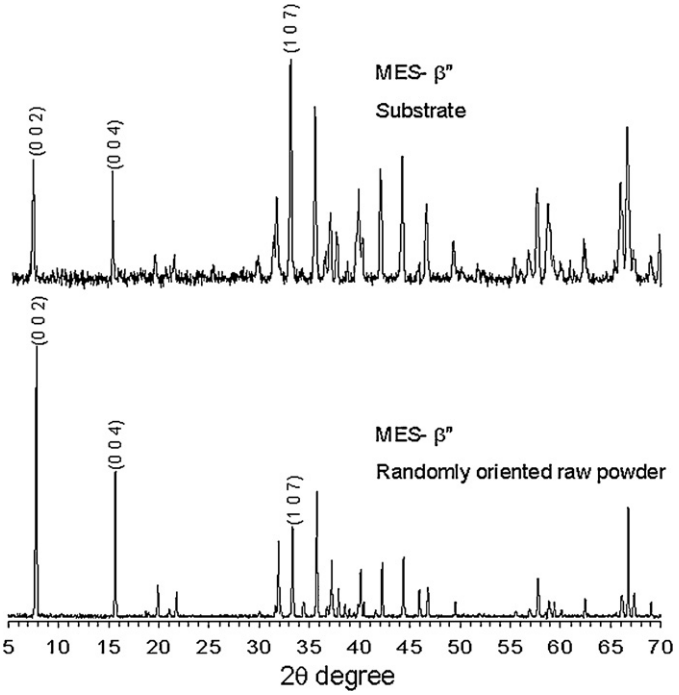

Fig. 10. Comparison between the X-ray diffraction patterns of MES-β″ powder and cast as the substrate.

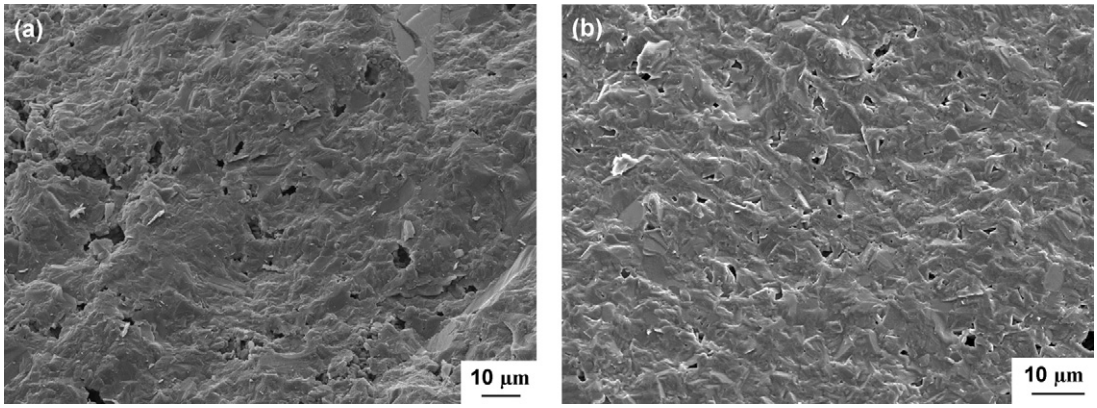

Fig. 11. SEM images of (a) pressed pellets of CMT-β″ sintered in buffer at 1650 °C for 30 min and (b) standard solid electrolyte of the Na/$NiCl_2$ (ZEBRA) cell.

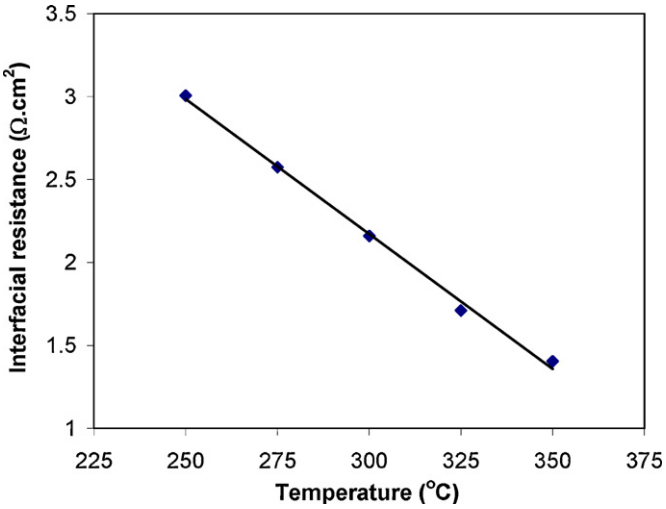

Fig. 12. Interfacial resistance of CMT-β″ pellets as a function of temperature measured by a Na|CMT-β″|Sn-1%Na cell.

3.2.2. Thin film electrolyte (≤50 μm)

Preliminary results of the resistance measurements of the hybrid solid electrolytes at 300 °C with a Na|CMT-β″ hybrid electrolyte|Sn-1%Na cell demonstrated a high specific resistance of near 42 Ω cm^2 for the hybrid electrolyte composed of CMT-β″ coating on a porous MES-β″ substrate. Such a high specific resistance could be assigned to the poor wetting of β″-alumina by liquid tin metal; as observed by SEM in the cells after testing, there was no trace of tin penetration into the substrate pores. In contrast, the wetting of β″-alumina by liquid sodium was observed to be significantly improved due to its lower viscosity (0.0167 N s m^{-2} [8] and 0.0035 N s m^{-2} [9] for Sn and Na, respectively at 300 °C).

The average specific resistance of the hybrid electrolyte measured by five Na|CMT-β″ hybrid electrolyte|Na cells was 1.60 Ω cm^2 which is lower than that for β″-alumina polished pressed pellets (2.61 Ω cm^2). This lower resistance could be explained by reduced thickness of the electrolyte coupled with an improved wetting of β″-alumina due to the capillary forces of the porous substrate. Assuming that the bulk resistance is attributed to only the 50 μm dense electrolyte coating, it can be concluded that nearly 80% of the electrolyte resistance arises from interfacial resistance, i.e., interfacial resistance is the dominant factor in the electrolyte resistance.

It is worth mentioning that the presence of gas bubbles encapsulated in the micro pores also plays a significant role to the overall electrolyte resistance. The entrapped bubbles impede the sodium mass transport to the thin film electrolyte. On the other hand, those bubbles remaining on the electrolyte surface decrease the efficient contact surface of the electrolyte resulting in a higher resistance. It is suggested that filling the cell in vacuum can be an effective method to remove the entrapped bubbles can reduce the overall electrolyte resistance.

4. Conclusions

Dense electrolyte tubes with a net thickness of less than 50 μm and supported on a porous substrate were successfully produced by slip casting. The porous substrates were prepared from β″-alumina with carbon powder as pore-forming agent in an aqueous slip. The coating slip consisted of β″-alumina dispersed in methanol. In contrast to other forming methods such as iso-static pressing which leads to an unfavorable texture, slip casting results in the thin film electrolyte consisting of randomly oriented grains which can improve the ionic conductivity.

The resistance of thin layer supported tubes versus full thickness electrolytes was tested by passing DC current through Na|β″-alumina|Na cell galvanic cells. The average specific resistance of the thin layer electrolyte cell was lower by a factor of 1.6. The components of cell resistance were determined. It was concluded that interfacial resistance is a dominant factor in the electrolyte resistance.

Acknowledgements

This work was supported by VALE INCO and by a grant from the Ontario Fuel Cell Research and Innovation Network. The authors acknowledge the contribution of personnel from the Canadian Center for Electron Microscopy and the Brockhouse Institute for Materials Research at McMaster University.

References

[1] J. Coetzer, J. Power Sources 18 (1986) 377–380.
[2] J.L. Sudworth, D.S. Dermott, R.C. Galloway, Electric Vehicles 73 (1987) 11–15.
[3] R.C. Galloway, J. Electrochem. Soc. 134 (1987) 256–257.
[4] H. Boehm, G. Beyermann, J. Power Sources 84 (1999) 270–274.
[5] D.W.J. Johnson, S.M.J. Granstaff, W.W. Rhodes, Am. Ceram. Soc. Bull. 58 (1979) 849–852.
[6] A. Pekarsky, P.S. Nicholson, Mater. Res. Bull. 15 (1980) 1517–1524.
[7] T. Oshima, M. Kajita, A. Okuno, Int. J. Appl. Ceram. Technol. 1 (2004) 269–276.
[8] A.J. Lewis, The absolute measurement of the viscosity of liquid tin, in: Proceedings of the Physical Society, vol. 48, 1936, pp. 102–110.
[9] Y.S. Chiong, Viscosity of liquid sodium and potassium, in: Proceedings of the Royal Society of London Series A, Mathematical and Physical Sciences, vol. 157, 1936, pp. 264–277.